Applied Surface Science 485 (2019) 255–265

Contents lists available at ScienceDirect

Applied Surface Science

journal homepage: www.elsevier.com/locate/apsusc

Full length article

Polarity on adsorption and photocatalytic performances of N-GR/TiO_2 towards gaseous acetaldehyde and ethylene

Xueping Dai[a,b], Yan Wang[a], Xiao Wang[a], Shengrui Tong[c], Xiaofeng Xie[a,*]

[a] Shanghai Institute of Ceramics, Chinese Academy of Sciences, 1295 Dingxi Road, Shanghai 200050, China
[b] University of Chinese Academy of Sciences, 19 (A) Yuquan Road, Beijing 100049, China
[c] Institute of Chemistry, Chinese Academy of Sciences, Beijing 100190, China

ARTICLE INFO

Keywords:
VOCs removal
Adsorption
Polarity
Photodegradation
Titanium dioxide

ABSTRACT

The surface adsorption is considered to be a very important factor in photodegradation process, especially in the removal of gaseous pollutants. In this work, nitrogen doped reduced graphene (N-GR)/TiO_2 were synthesized to probe the polarity adsorption and photodegradation characteristics of acetaldehyde (polar) and ethylene (nonpolar). Morphology and properties of the samples were revealed by TEM, Raman spectra, photoluminescence spectra, photocurrent, electron spin resonance and so forth. Adsorption of flowing gas and TPD were used to indicate the adsorption ability of the composites towards acetaldehyde and ethylene. In experiments, the difference of nitrogen doping amount can adjust the polarity of N-GR/TiO_2 composites efficiently and then influence their photodegradation performance. Specifically, the N-GR/TiO_2 showed higher acetaldehyde adsorption capacity than GR/TiO_2, while the GR/TiO_2 possessed the highest adsorptive abilities in ethylene case. In the subsequent photodegradation tests of flowing acetaldehyde, all of the N-GR/TiO_2 samples had removal efficiencies higher than that of GR/TiO_2. The highest removal efficiency reached by the 2 N-GR/TiO_2 is around 82%. In the ethylene to contrast, the removal efficiency was obtained as 93.8% by GR/TiO_2, which is higher than that of the N-doped samples. It can be seen that the high polarity samples could improve the adsorption and photodegradation performance of polar molecules, which could propel the understanding and application of photodegradation technologies.

1. Introduction

The removal of volatile organic compounds (VOCs) has drawn more and more attention [1,2], since they not only can cause terrible human disease [3,4], but also can react with NO_X, SO_2 and accelerate the formation of secondary organic aerosol (SOA) as well as $PM_{2.5}$ particles through complex heterogeneous reaction [5,6]. It has been proved that TiO_2 photocatalyst can effectively remove VOCs and inhibit the generation of SOA according to a serial of photocatalytic reactions [7]. However, the unsatisfied photodegradation performance of commercial TiO_2 prevent it from being widely applied [8–11]. It was revealed that the adsorption ability of TiO_2 has an important impact on their removal efficiency towards gas pollutants [12,13]. Furthermore, the high flowing speed of the gas pollutants would inevitably increase the difficulty of capturing them [14,15]. After all, only the gas molecules captured by photocatalyst surface can be oxidized and then eliminated in the photocatalytic process [12,16,17].

So far, many efforts have been put into enhancing the adsorption ability of the photocatalysts [18]. One way of enhancing the adsorption of gas volatile molecules is to create more specific surface areas (SSA) either by constructing multiple-scale microstructure [19–21] or by coupling with other materials with high SSA [13,22,23]. Another way is to modify the surface affinity of photocatalyst towards target molecules according to the principle “like dissolves like”. To be specific, gas molecules prefer to interact with the photocatalysts with a similar structure or polarity [21,24,25]. Zahra et al. fabricated fluorine modified TiO_2 (F-TiO_2) nanoparticles and found that F-TiO_2 could adjust the hydrophobicity of TiO_2 and better enhance the adsorption of non-polar molecules like toluene than polar molecules such as isobutanol toluene [26]. Thanh-Dong et al. also found that the surface of photocatalyst was more occupied by high polar butyl acetate rather than nonpolar hexane in the mixture stream [27]. Nowadays, the interaction between target organic molecules and photocatalyst have drawn more and more attention [28,29]. Accordingly, it is quite meaningful to reveal the polarity effects on the adsorption and photodegradation of typical polar and nonpolar VOCs pollutants.

* Corresponding author.
E-mail address: xxfshcn@163.com (X. Xie).

https://doi.org/10.1016/j.apsusc.2019.04.221
Received 14 February 2019; Received in revised form 14 April 2019; Accepted 24 April 2019
Available online 24 April 2019
0169-4332/ © 2019 Elsevier B.V. All rights reserved.

Recently, graphene was often introduced to improve the adsorption abilities and photon-generated electrons transmission of photocatalysts [30–32]. In our previous work graphene was coupled with TiO_2 and the adsorption ability towards acetaldehyde and o-xylene was improved a lot [33]. Furthermore, some researches adopted nitrogen-doping method to obtain better photodegradation performance of graphene composite photocatalysts [34,35]. Mou et al. [36] found that the nitrogen doped graphene(N-GR) could improve the efficiency of the photoinduced charges' transfer and separation on the composite. Xu et al. [35] proposed that nitrogen doped graphene could not only serve as an effective electron-transfer mediator but also function as the oxygen-reduction active sites. Most of the work about N-GR/TiO_2 concentrates on the role of the nitrogen atoms play in the photocatalytic process. Actually, nitrogen doped graphene not only has the great SSA but also has stronger polarity [37] and more functional groups than graphene [38–40], which could make a difference on the capture of VOCs. However, there are only a few attention given to the effects of N-doped graphene on the adsorption ability of those composites.

In this work, the adsorption abilities of N-GR/TiO_2 towards acetaldehyde and ethylene and the subsequent influences on their photodegradation process have been investigated systematically. Acetaldehyde and ethylene were thought as two of the typical industrial VOCs pollutant. They are both carcinogenic and very common in daily life [16]. Besides, their simple structure (both possess two carbon atoms) and different polarity make them good candidates for detecting the influence of polarity on the adsorption and photocatalytic performances. This work could provide a strategy for selective adsorption and removal of VOCs pollutants.

2. Experimental

All chemical agents, including commercial TiO_2 (Degussa P25, containing 70% anatase and 30% rutile), graphite, dicyandiamide (DCDA, purchased from Aladdin), H_2SO_4 (98%, Sinopharm), H_3PO_4 (85%, Sinopharm), hydrochloric acid (HCl, 37%, Sinopharm), $KMnO_4$ (Alfa), H_2O_2 (30 wt%, Sinopharm) and ethanol (supplied by Sinopharm Chemical Reagent CO., Ltd.) were used as received without any further purification.

2.1. Preparation of samples

GO was synthesized by a modified Hummer's method [40]. Typically, 0.75 g natural graphite flake (Alfa) was added in 90 ml H_2SO_4 (98%, Sinopharm) and then 10 ml H_3PO_4 (85%, Sinopharm) was added dropwise. The suspension was vigorously stirred in ice-water bath, the temperature of which should be kept lower than 5 °C. Then $KMnO_4$ (99%, 4.5 g, Alfa) was added slowly in the suspension (attention: $KMnO_4$ should be added carefully and slowly, otherwise, too much heat can easily cause explosion) and the suspension was kept stirring overnight. 10 ml H_2O_2 (30 wt%, Sinopharm) was further added dropwise. After being stirred for another 12 h, the obtained bright yellow suspension became dark brown. Finally , dialysis was used to move remained acid and GO suspension was prepared.

N-GR/TiO_2 composites were prepared by a simple heat treatment method. Firstly, 1 g TiO_2 was put into 40 ml deionized water (DI) by sonication. Then 500 μl HCl (37 wt%, Sinopharm) was added and the suspension was stirred continuously. 10 ml GO suspension (1 mg/ml) was later slowly added into TiO_2 suspension. The surface potential of GO is always negative while TiO_2 gets a positive surface potential when pH is lower than 2 [33], which is very important for the coupling of GO with titanium dioxide. The mixed suspension was stirred for 6 h to make sure TiO_2 nanoparticles are coupled with GO completely. Then the suspension was heated to remove HCl and get dry powder. The powder was next washed by DI water and ethanol for 3 times. 0 mg, 10 mg, 20 mg, 30 mg DCDA was dissolved in 20 ml ethanol respectively, followed by mixing with GO/ TiO_2 powder (the samples were marked as GR/TiO_2, 1 N-GR/TiO_2, 2 N-GR/TiO_2, 3 N-GR/TiO_2). Finally, the powder was put into the muffle and being calcinated at 350 °C for 3 h, with a heating rate of 5 °C/ min.

2.2. Characterization

The microstructure and morphology was revealed by transmission electron microscopy (TEM, JEM-2100F). The X-ray diffraction (XRD) spectra were measured using an X-ray diffractometer (Ultima IV 2036E102, Rigaku Corporation, Japan). DXR Raman Microscope (Thermal Scientific Corporation, USA) was used to record Raman spectra. The zeta potential was measured by Zetaplus (Brookhaven Instruments). Specifically, 0.02 g sample was dispersed in 200 ml deionized water with ultrasonic bath for 5 min. 1 ml KCl solution (1 mol/L) was added into the suspension to improve the conductivity of the suspension. HCl or NaOH solution was used to adjust the pH of this suspension to desired values. The average value of the potential after ten cycles was recorded.

UV − vis diffuse reflectance spectra was obtained on Shimadzu UV-3600 spectrometer. Fourier transform infrared (FTIR) spectra was carried out by a Thermal Scientific 5225 Verona Rd using KBr as reference. Photoluminescence (PL) spectra was recorded by an Edinburgh Instruments FLSP-920 fluorescence spectrophotometer with an excitation wavelength of 320 nm. Microlab 310F scanning Auger microprobe (VG Scientific Ltd) was used for X-ray photoelectron spectroscopy (XPS) analysis. Photocurrent measurement was performed on a CHI 660B potentiostat/galvanostat electrochemical analyzer with a typical three-electrode configuration system, with the prepared samples as the working electrode, a saturated calomel as a reference electrode, and a platinum sheet as a counter electrode. The electrolyte was 1 mol/L NaCl aqueous solution. The transient photocurrent was recorded while the working electrode was irradiated with a chopped illumination by a 150 W xenon lamp. The JES-FA200 spectrometer was applied to detect the electron spin resonance (ESR) signals of radicals, with the radicals trapper 5,5-dimethyl-1-pyrroline N-oxide (DMPO). Before ESR detection, 0.02 g sample was dispersed in 1 ml DI water (for •OH detection) or ethanol(for $\bullet O_2^-$ detection), into which pure O_2 was bubbled for 10 min. Then the dispersion was exposed under a 150 W xenon lamp for 5 min.

2.3. Adsorption and desorption detection

Temperature programmed desorption (TPD) analysis was performed by ChemiSorb PCA-1200 (Builer, China). During the test, 0.1 g of the sample was placed in a quartz tube, which was heated at 393 K by an electric furnace for 1 h in high-purity nitrogen gas in order to obtain a clean TiO_2 surface. After cooling down to room temperature, acetaldehyde (or ethylene, respectively) flowed through the sample tube with a rate of 20 ml/min for 2 h to reach adsorption equilibrium. Finally , the temperature was raised at a rate of 10 K/min to 873 K under the protection of nitrogen. At the same time Thermal Conductivity Detector (TCD) was used to detect the desorption signal of acetaldehyde (or ethylene). Dark adsorption detection was carried out by a real-time monitoring system, as showed in Fig. 1, which contained three parts: gas mixer, reaction cell and gas chromatograph (CEAULIGHT, GC-7920) with capillary column. The real-time concentration of the gas was recorded by GC.

2.4. Photocatalytic performance detection

Photodegradation test was carried out in the same system with dark adsorption detection. 0.1 g photocatalyst was dispersed in ethanol and then uniformly coated on a glass pane (15 cm × 7.5 cm × 3 mm). During the test, the sample coated glass pane was placed in the reaction chamber sealed with a quartz glass. Air provided by air generator was

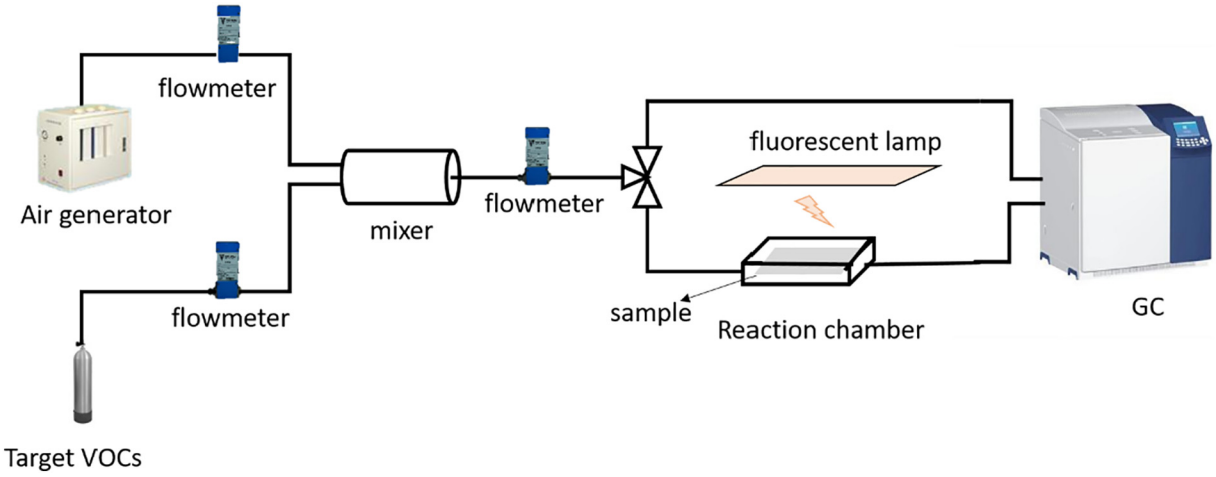

Fig. 1. Real-time monitoring system for the adsorption and photodegradation.

mixed with target VOCs in the gas mixer and then flowed through the reaction chamber to GC. The initial concentration of acetaldehyde was 500 ppm while the initial ethylene was 50 ppm. The flowing rate of acetaldehyde and ethylene were both 20 sccm. The light source for acetaldehyde was fluorescent lamp with a power of 260 W while for ethylene was Xenon lamp with a power of 500 W. The dark adsorption detection was also carried out in this system.

3. Results and discussion

3.1. Characterization of morphology and chemical composition

Fig. 2a and b show the HRTEM images of N-GR/TiO_2. TiO_2 nanoparticles dispersed on the N-doped graphene nanosheets homogeneously. The size of the nanaoparticles was around 20–30 nm in diameter. Fig. 2b clearly shows the lattice fringe of TiO_2. The interplanar spacing of 0.35 nm belongs to the (101) plane of anatase TiO_2, while 0.29 nm was the interplanar spacing of the (001) plane of rutile TiO_2 [41]. However, in the XRD spectra (Fig. 2c) no graphene peak or N-doped graphene peak was shown, which was due to the fact that the concentration of graphene (less than 1 wt%) did not reach the XRD detection limit. The characteristic diffraction line of anatase and rutile phases had no change after the compositing treatment, meaning that heat treatment had no influence on the crystal structure of the TiO_2 nanoparticles. The FTIR spectra (Fig. 2d) revealed that the nitrogen atoms were definitely doped in the graphene. The peaks at 592 cm^{-1}(O-Ti-O), 1628 cm^{-1}(C = O), 3402 cm^{-1}(O—H) were assigned to the pristine TiO_2, GR/TiO_2 and N-GR/TiO_2, due to the inevitable adsorption of CO_2 and H_2O molecules on the surface of the samples. Both GR/TiO_2 and N-GR/TiO_2 had a peak at 2358 cm^{-1} (C = C), assigned to the carbon structure of graphene. The particular peaks of N-GR/ TiO_2 sample appeared at 2308 cm^{-1}, 2332 cm^{-1}, 2857 cm^{-1}, 2924 cm^{-1}, which were ascribed to C—N and N—H vibration peaks.

Zeta potential was used to indicate the polarity of the samples. Fig. 3(a) showed that the 2 N-GR/TiO_2 had larger absolute value of the potential than GR/TiO_2 at the same pH, which indicated that the polarity of the sample was improved after nitrogen doped. Raman spectroscopy is a powerful tool to investigate the structure of carbon materials. Fig. 3b was the Raman spectra and partial enlarged drawing of the spectra. A decrease in the ratio of the D band (ca. 1350 cm^{-1}) and G band (ca. 1600 cm^{-1}) intensities (I_D/I_G) was observed after the heat treatment, indicating the effective reduction of GO and the formation of GR/TiO_2 [42]. The I_D/I_G of N-GR/TiO_2 was higher than that of both GO/TiO_2 and GR/TiO_2, due to a broken hexagonal symmetry of the graphene structure, which could also demonstrate that N atoms were doped in graphene sheets [43]. Interestingly, the color of the samples, as showed in Fig. 3c, changed with the treatment method. The color of GO/TiO_2, without any heat treatment, was brown and that was mostly the color of graphene oxide. After the heat treatment in the muffle for 3 h , the sample without DCDA became light gray, as a result of the reduction of graphene and the loss of some GO. In contrast, the samples with DCDA were dark gray, revealing that the nitrogen doped process could reduce the loss of graphene in heat treatment.

XPS spectra (Fig. 4a–d) further reveals the interaction of the components. Fig. 4b is the C1s spectra of GR/TiO_2 and 2 N-GR/TiO_2. The three peaks of the C1s spectra were ascribed to sp^2 bonded carbon (C—C, 284.8 eV), epoxy (C—O, 286.5 eV), carbonyls (C═O, 288.5 eV) [44]. Due to the fact that the binding energy of C═O and C—N are both around 288 eV, the higher peak around 288.5 eV of 2 N-GR/TiO_2 than that of GR/TiO_2 was caused by the overlay of C═O and C—N peaks. Compared with pristine TiO_2, Ti 2p spectra (Fig. 4c) of the GR/TiO_2 and 2 N-GR/TiO_2 both had a certain shift to higher binding energy(Ti 2p3/2 changes from 458.32 eV to 458.60 eV and 458.62 eV, respectively), resulting from the interaction of Ti-O-C bond [45]. However, the binding energy of Ti 2p of the GR/TiO_2 and 2 N-GR/TiO_2 sample almost had no difference, disclosing that there was no direct interaction between N atoms and Ti or O atoms of TiO_2. The N 1 s spectra of 2 N-GR/TiO_2 shows peaks at 401.19 eV and 399.67 eV, referring to the quaternary and pyrrolic N atoms respectively. This result was in line with the FTIR spectra. To be specific, the quaternary N atoms contribute to C—N bonds while the pyrrolic N atoms make for N—H bonds. Since the peak area of pyrrolic nitrogen was higher than that of quaternary nitrogen, it was reasonable to claim that most of the doped nitrogen atoms were in the form of pyrrolic nitrogen. In previous work, pyrrolic N atoms were proved to function as the oxygen-reduction active sites and promoted the interfacial catalytic reaction while the quaternary N atoms were effective electron mediators [35], which both facilitated the photodegradation of the organic molecules.

3.2. Adsorption capacity of the composite

For the photodegradation of gaseous contamination, capture of the organic molecules would be a very important step [20]. There are two kinds of adsorption, including physical adsorption and chemical adsorption. Specific surface areas indicate the physical adsorption ability of the samples and was revealed by the BET model (Table 1) in this work. Interestingly, the S_{BET} decreased with the treatment of coupling. Pristine TiO_2 had S_{BET} as large as 68.01 m^2/g, while that of GR/TiO_2 is 55.21 m^2/g. For N-GR/TiO_2, with the increasing of the content of nitrogen, S_{BET} decreased from 50.65 m^2/g (1 N-GR/TiO_2) to 45.29 m^2/g (3 N-GR/TiO_2). The reason could be that the heat treatment and DCDA could promote the agglomeration of TiO_2 nanoparticles.

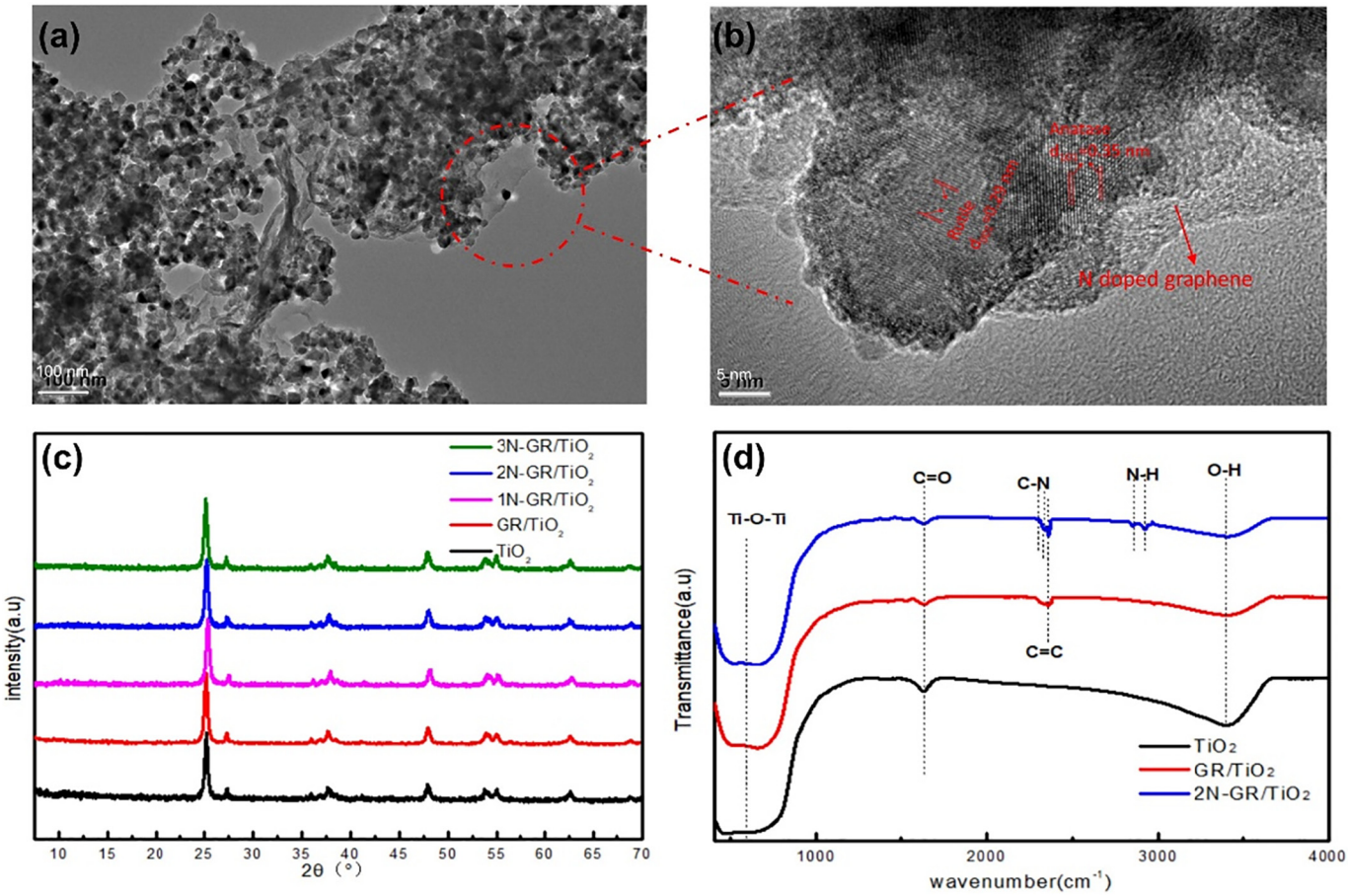

Fig. 2. Morphological and structure characterization of the samples. (a) TEM image and (b) HRTEM image of selected area of 2 N-GR/TiO_2 sample; (c) XRD spectra of pristine TiO_2, GR/TiO_2 and N-GR/TiO_2 with different doped nitrogen content; (d) FTIR patterns of pristine TiO_2, GR/TiO_2 and 2 N-GR/TiO_2.

Diametrically opposite to the trend of S_{BET}, the adsorption amount of acetaldehyde increased with the presence of graphene and doping amount of nitrogen. Fig. 5a shows real-time concentration of acetaldehyde in the reaction chamber. The adsorption amount of the target gas could be calculated by the equation:

$$V_{adsorption} = \left(\int_0^t \nu \times c_t dt\right)_{blank} - \left(\int_0^t \nu \times c_t dt\right)_{sample} = \nu\left(\int_0^t (c_t)_{blank} - (c_t)_{sample}\right)$$

υ is the flowing speed of the gas and the c_t is the real-time concentration of the reaction chamber. The enclosed area of the baseline C/C_0 = 1 and the curve could indicate the amount of absorbed

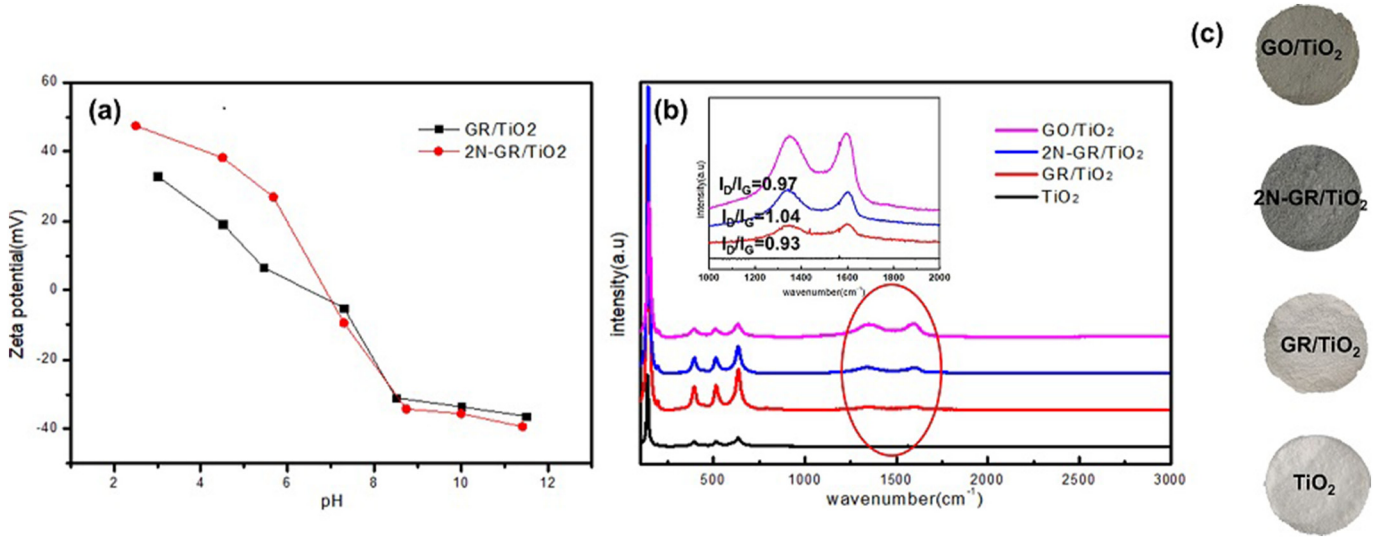

Fig. 3. (a) Zeta potential of 2 N-GR/TiO_2 and GR/TiO_2 at different pH (b) Raman spectra and (c) pictures of the TiO_2, GR/TiO_2, 2 N-GR/TiO_2 and GO/TiO_2.

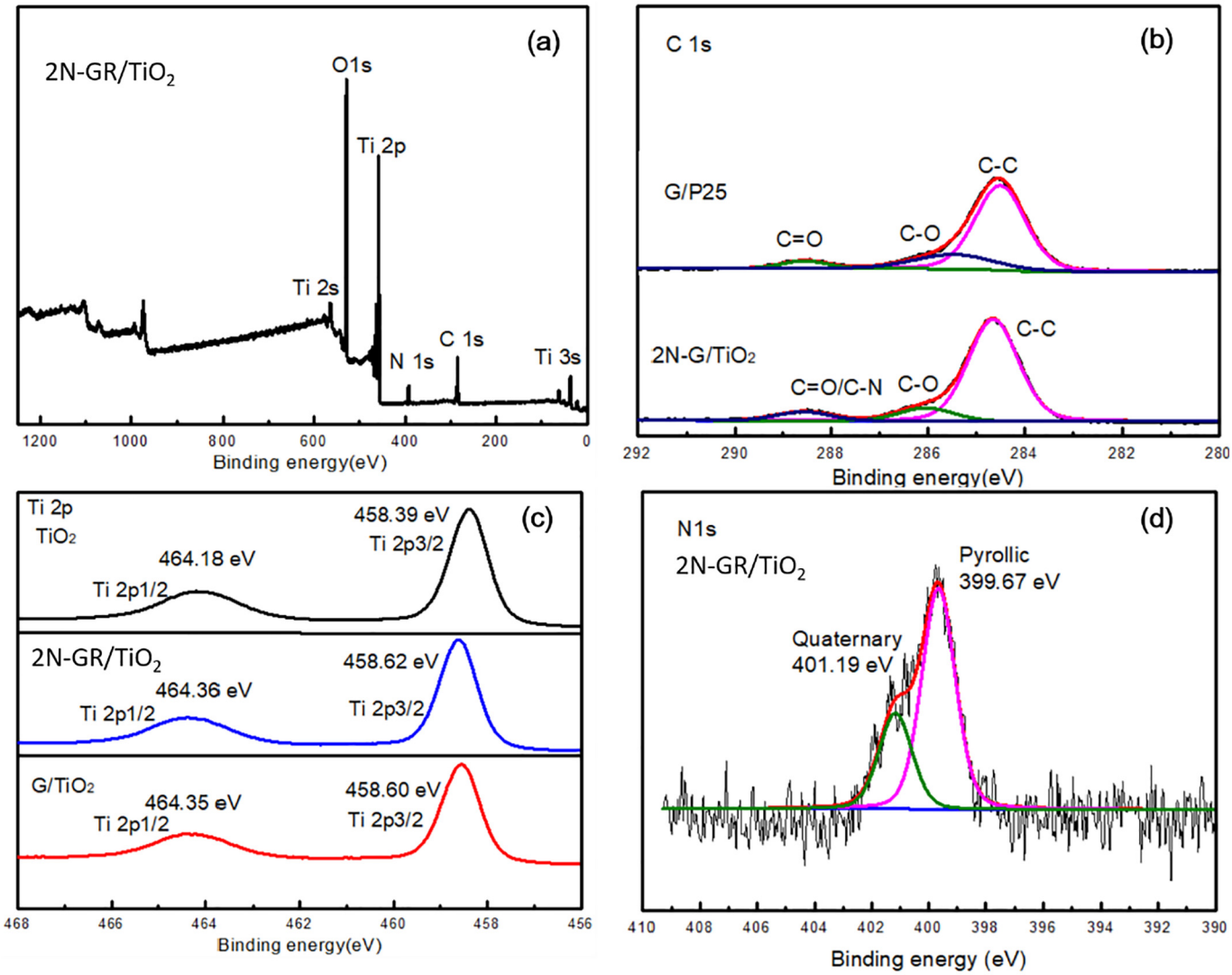

Fig. 4. (a) XPS survey spectrum and (d) N1 s spectra of 2 N-GR/TiO_2 composite; (b) C 1 s spectra of GR/TiO_2 and 2 N-GR/TiO_2 composite; (c) Ti 2p spectra of pristine TiO_2 and GR/TiO_2, 2 N-GR/TiO_2.

Table 1
The specific surface area of the samples calculated by BET method.

Sample	TiO_2	GR/TiO_2	1 N-GR/TiO_2	2 N-GR/TiO_2	3 N-GR/TiO_2
$S_{BET}(m^2/g)$	68.01	55.21	50.65	46.89	45.29

acetaldehyde. When coupled with graphene, especially nitrogen doped graphene, the adsorption amount increased a lot. The 3 N-GR/TiO_2 sample even had four times as much acetaldehyde adsorption amount as the pristine TiO_2 sample. Fig. 5c is the TPD spectra of acetaldehyde, the area of whose peak was used to reveal the adsorption capacity of the samples. Obviously, the desorption peak of 2 N-GR/TiO_2 sample was higher than both GR/TiO_2 sample and the pristine TiO_2. It was reasonable to deduce that the nitrogen doped graphene could improve the adsorption amount of acetaldehyde, arising from that the doped N atoms could improve the polarity of graphene. Besides, the pyrrolic N atoms could form amidogen (-NH_2), a group which has affinity towards aldehyde group (-CHO) [46,47]. Nucleophilic addition could easily happen between amidogen and aldehyde group and yield Schiff base [48,49]. Compared with pristine TiO_2 and GR/TiO_2, the desorption peak of 2 N-GR/TiO_2 showed a distinct shift to higher temperature (about 20 °C shift), which could stem from the affinity between -NH_2 and –CHO. Different from acetaldehyde, the adsorption amount of ethylene (Fig. 5b) did not have a positive correlation with the increasing amount of nitrogen in N-GR/TiO_2. In fact, the higher content of doped nitrogen in composites, the less ethylene was captured. GR/TiO_2 had the best adsorption ability towards ethylene, which was more than 5 times of the amount of pure TiO_2. The sample 3 N-GR/TiO_2 almost had the same adsorption amount of ethylene with pristine TiO_2. Fig. 5d shows the TPD spectra of ethylene. There was not much difference between the curves of sample GR/TiO_2 and 2 N-GR/TiO_2. The sample GR/TiO_2 and 2 N-GR/TiO_2 had three peaks at 150 °C, 250 °C and 330 °C, while pristine TiO_2 only had two peaks at 150 °C and 310 °C. It was attributed to that carbon atoms of the composition introduced more adsorption sites towards ethylene. However, the doped nitrogen atoms promoted the polarity of graphene structure, which had negative effect on the adsorption of nonpolar ethylene molecules. From the TPD and flowing gas detection, it was found that compared with GR/TiO_2, nitrogen doped graphene/TiO_2 composites could promote the adsorption of polar acetaldehyde while weaken the adsorption capacity of nonpolar ethylene.

3.3. Photocatalytic performance and photoelectric properties

Fig. 6a and b show the photodegradation performance of the

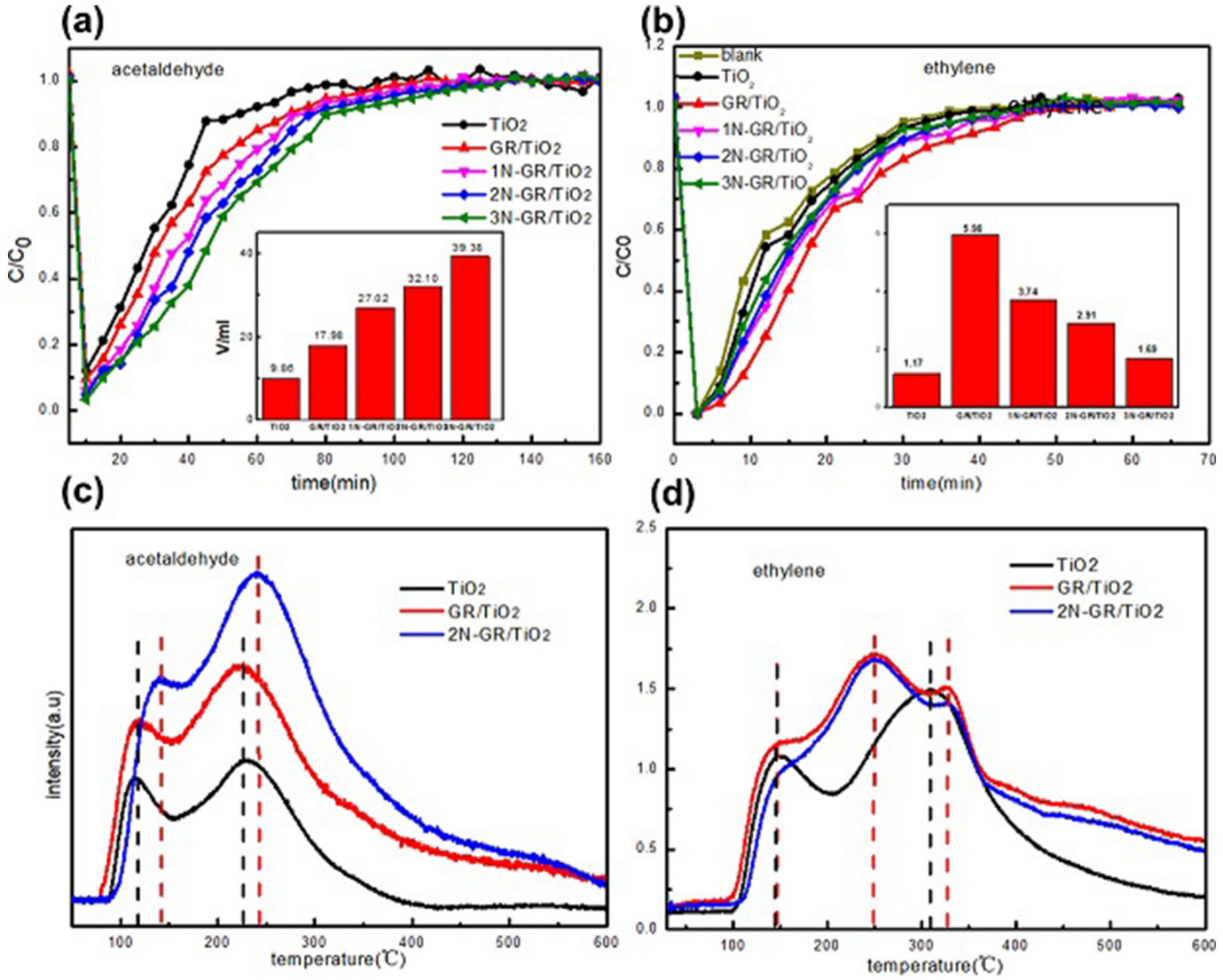

Fig. 5. Adsorption of flowing (a) acetaldehyde and (b) ethylene detection; TPD spectra of (c) acetaldehyde and (d) ethylene. The flowing rate of acetaldehyde and ethylene was both 20 sccm. Initial concentration of acetaldehyde was 500 ppm while initial concentration of ethylene is 50 ppm.

samples towards acetaldehyde and ethylene. The initial concentrate of acetaldehyde was 500 ppm and the flowing speed was 20 sccm. Both acetaldehyde and ethylene could not be degraded by merely illumination without photocatalyst. As shown in Fig. 6a, 2N-GR/TiO_2 sample had the best photocatalytic ability towards acetaldehyde, followed by the other N-GR/TiO_2 samples. All the N-GR/TiO_2 samples had removal efficiencies higher than 72%, better than that of GR/TiO_2 (about 70% at a stable state). The highest removal efficiency reached by the 2 N-GR/TiO_2 was around 82%, with twice enhancement than that of pristine TiO_2. The GR/TiO_2 sample also reached a degradation efficiency of 70.6%, since the coupling of graphene could improve the separation of electrons and holes, as well as the adsorption of pollutant molecules. However, too much dopant did not result in best photodegradation ability. The 3 N-GR/TiO_2 had lower photodegradation ability than 2 N-GR/TiO_2 and 1 N-GR/TiO_2. The removal efficiency of ethylene were also detected under Xenon lamp (Fig. 6b). Since breaking the carbon-carbon double bond (C = C) needs higher energy [50–52], the Xenon lamp with similar emitting spectrum to sunlight and greater light intensity was used for ethylene degradation. Initial concentration of ethylene was 50 ppm and the flowing speed was 20 sccm. The highest removal efficiency of ethylene was 93.8% by GR/TiO_2, almost double that of pristine TiO_2 (50.1%). All N-GR/TiO_2 samples showed photodegradation efficiency around 90%, lower than that of GR/TiO_2. Comparing the adsorption and removal efficiency of acetaldehyde and ethylene, conclusion could be drawn that doped nitrogen atoms could promote the removal efficiency of polar molecules by improving the adsorption of them.

Considering the adsorption and photocatalytic ability of the samples, the photoelectric properties and the yield of radicals were used to further unravel the background mechanism. UV–vis absorption and photoluminescence (PL) spectra were used to detect the utility efficiency of photo energy. The former revealed the adsorption of the incident light and the latter unraveled the combination of the photogenerated carriers. From Fig. 7a and b, an improvement of UV–vis absorption and a reduction of PL intensity were observed with the addition of graphene and nitrogen doped graphene, which could be attributed to that graphene and N-doped graphene acted as photoelectron acceptors, preventing the electrons and holes from recombination. The photocurrent response showed that the GR/TiO_2 sample had the highest current density(15.47 μA/cm^2), which was about twice higher than that of pristine TiO_2 (5.42 μA/cm^2). The photocurrent response of all N-GR/TiO_2 samples were lower than that of the GR/TiO_2 while higher than that of pristine TiO_2, which was different from the previous work [34,36,53,54]. This phenomenon could be explained by Ferrighi's

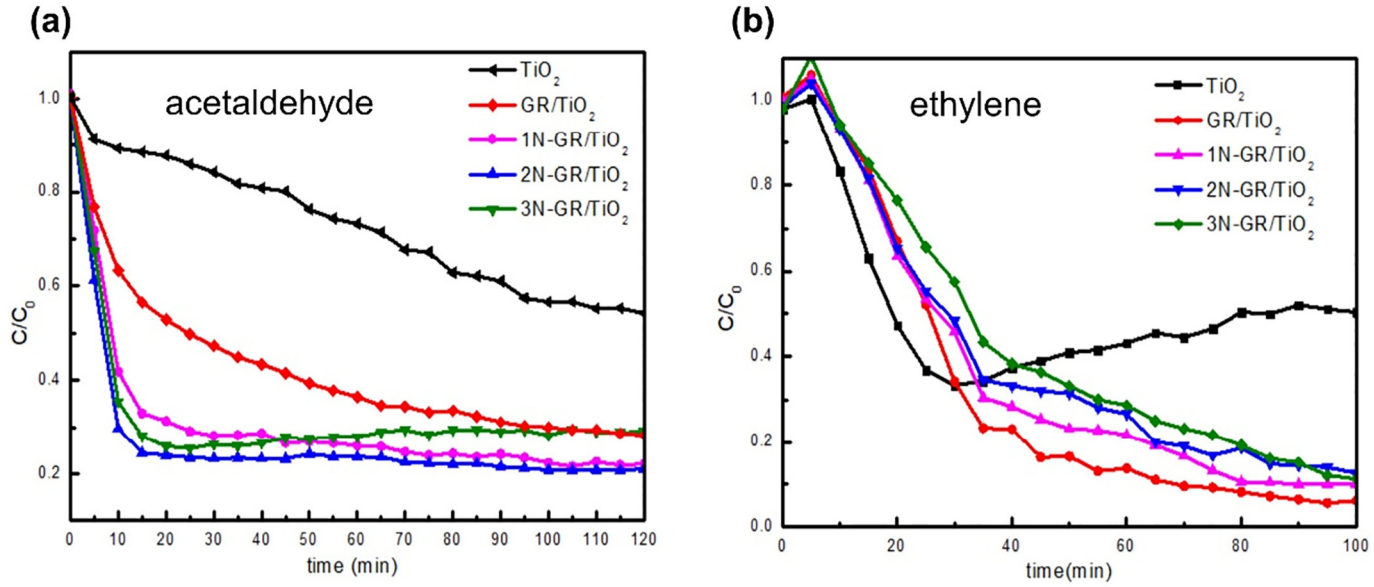

Fig. 6. photodegradation efficiency of the samples towards (a) acetaldehyde and (b) ethylene. Initial concentration of acetaldehyde was 500 ppm, while initial concentration of ethylene was 50 ppm. Flowing speed of them were both 20 sccm.

calculation that the doped nitrogen atoms provided extra electron to fill the delocalized p band of graphene and N-GR/TiO_2 had higher Fermi level than GR/TiO_2 [55]. The band gap between the conduction band and the valence band could be opened by the doped nitrogen atoms [38,39]. It would be harder for the photoelectrons on TiO_2 to transfer to N-doped graphene. Besides, the high content of pyrrolic nitrogen indicated that the integrity of graphene had been broken, which would reduce its electrical conductivity and diminish the photocurrent response of N-GR/TiO_2 samples. Since more doped nitrogen amount leaded to the larger bandgap of N-GR and more severe destruction of the graphene structure, when the doping amount of nitrogen atoms increased, the photocurrent intensity decreased (Fig. 7c).

Electron spin resonance (ESR) was used to detect the production of the active species such as hydroxyl radical (·OH) and superoxide radicals ($\cdot O_2^-$). To the best of our knowledge, ESR signal is usually detected in liquid phase [56], where there are little oxygen molecules. In order to get near to the air environment, oxygen was bubbled into the supension of the sample. Unlike the photocurrent graph, the strongest signal of both $\cdot O_2^-$ and $\cdot OH^-$ occurred in 2 N-GR/TiO_2 sample, which was much higher than that of the GR/TiO_2 sample (Fig. 8). There is almost no signal of ·OH and the weakest $\cdot O_2^-$ on the pristine TiO_2, since electrons and holes are easy to combine on the TiO_2 surface, leading to low production of active species [57]. The inconformity of photocurrent and ESR signals could be attributed to two mutual suppression factors. On one hand, more doped nitrogen atoms mean more terribly broken graphene structure and more enlarged band gap, as a result of which less photoelectrons could transfer to the N-G successfully. On the other hand, the increased amount of doped N atoms would be quite favorable for O_2 adsorption [58] and electrons were more likely to transfer to oxygen molecules to generate $\cdot O_2^-$ on the N atoms [55]. In other words, although the 2 N-GR/TiO_2 sample was not the one that had the most electrons transferring to N-G, it was the sample that most of the photo-induced electrons combined with oxygen molecules and yielded most active radicals.

3.4. Mechanism of enhanced adsorption and photocatalytic activity

On the basis of the holistic detection, a proper mechanism was proposed to explain the improvement of photocatalytic performance. Photocurrent, PL spectra and radicals detection could confirm that the recombination of the photogenerated charges of TiO_2 were prevented by coupling with nitrogen doped graphene. Besides, more active radicals including $\cdot O_2^-$ and ·OH were yielded on the sample of 2 N-GR/TiO_2. Most importantly, the adsorption ability was greatly improved by coupling with a certain ratio of nitrogen doped graphene.

Adsorption process was the first step. As shown in Fig. 9a, for the pristine TiO_2, both adsorption and oxidation were very slow, arising from the poor ability of capturing pollutants and low yield of active radicals. When coupled with graphene, organic molecules were inclined to adhere on the surface of the composite, resulting a promotion in the adsorption efficiency. Interestingly, the outstanding adsorption ability did not come from higher specific surface area (S_{BET}) of the two dimensional structure of graphene. The improved adsorption capacity for acetaldehyde could be explained from two aspects: on one hand, the doped nitrogen could improve the polarity of graphene [37,59], which lead to more polar molecules captured by electrostatic force; on the other hand, the amidogens formed on pyrrolic nitrogen atoms had strong affinity to aldehyde groups. In contrast, the N-GR/TiO_2 had no advantage over GR/TiO_2 in adsorption of ethylene since ethylene has no polarity. Totally, introduction of graphene could improve the adsorption of organic molecules and improving polarity of graphene could further promote the adsorption of polar organics.

In the photodegradation process, as shown in Fig. 9b, electrons of the valance band adsorb the energy of photons and jump to the conduction band [60], and then transfer to the surface of graphene or nitrogen doped graphene [61]. The quaternary nitrogen atoms act as electrons transferring medium and the pyrrolic nitrogen atoms serve as the actives sites [62], where oxygen atoms get electrons and yield super oxygen radicals. The remained holes on TiO_2 react with adsorbed water molecules and produce hydroxide radicals [30,63]. When the organic molecules are captured by the photocatalyst, acetaldehyde is firstly oxidized into acetic acid and then into carbon dioxide and water [15,33], the leading radicals are mainly $\bullet O_2^-$ [14,15]. In the ethylene photodegradation process, the whole reaction is more caused by •OH [64]. Ethylene is firstly oxidized into formaldehyde and then under the cooperation of •OH and $\bullet O_2^-$ into CO_2 and H_2O. Since $\bullet O_2^-$ does not make the leading influence on the degradation of ethylene [65,66], it is reasonable for the N-GR/TiO_2 composites, while produce more super oxide radicals, show lower photocatalytic ability in the removal of ethylene than that of GR/TiO_2 composite.

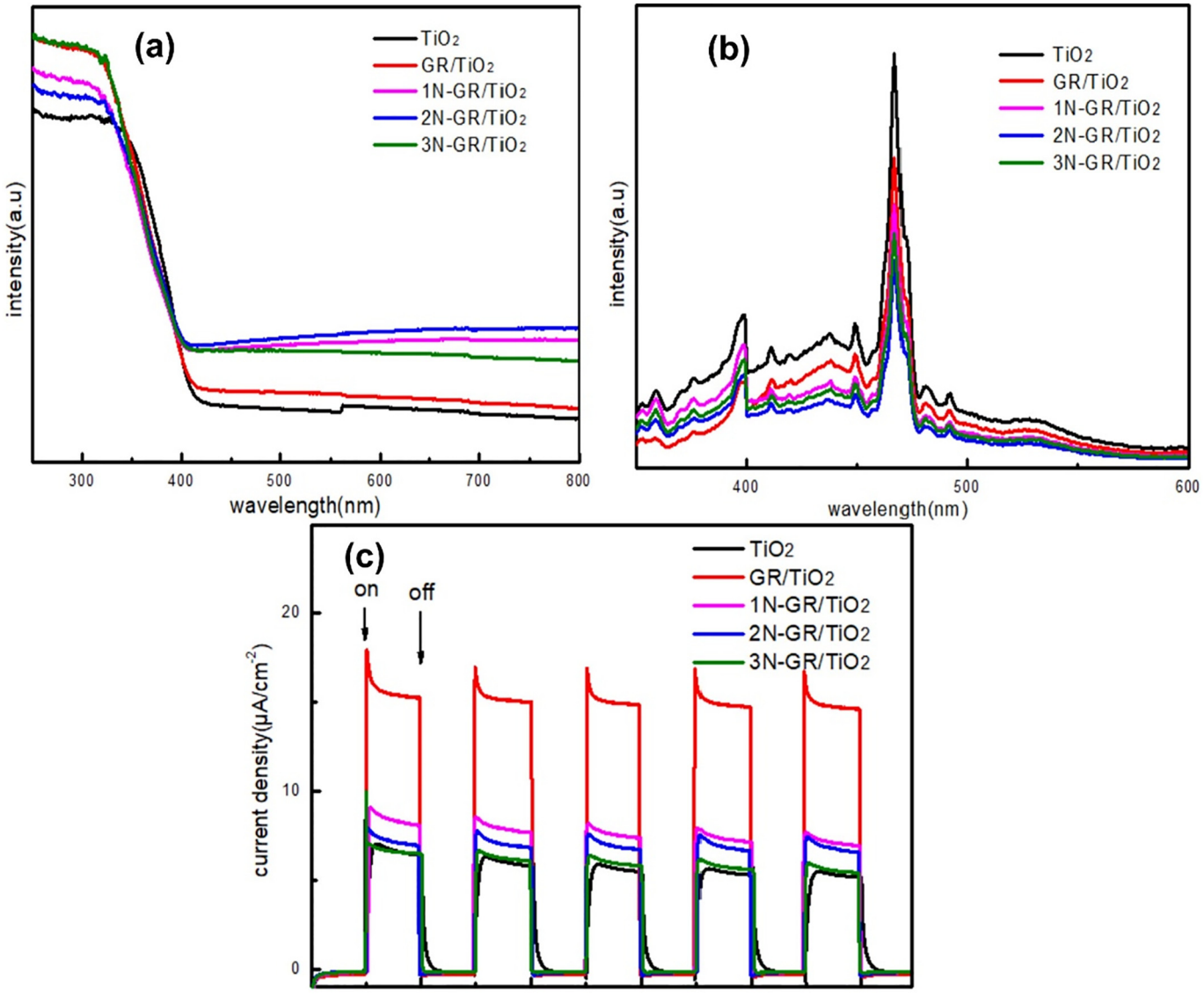

Fig. 7. (a) UV–Vis adsorption spectra and (b) photoluminescence spectra, (c) photocurrent response of pristine TiO_2 and GR/TiO_2, 1 N-GR/TiO_2, 2 N-GR/TiO_2, 3 N-GR/TiO_2.

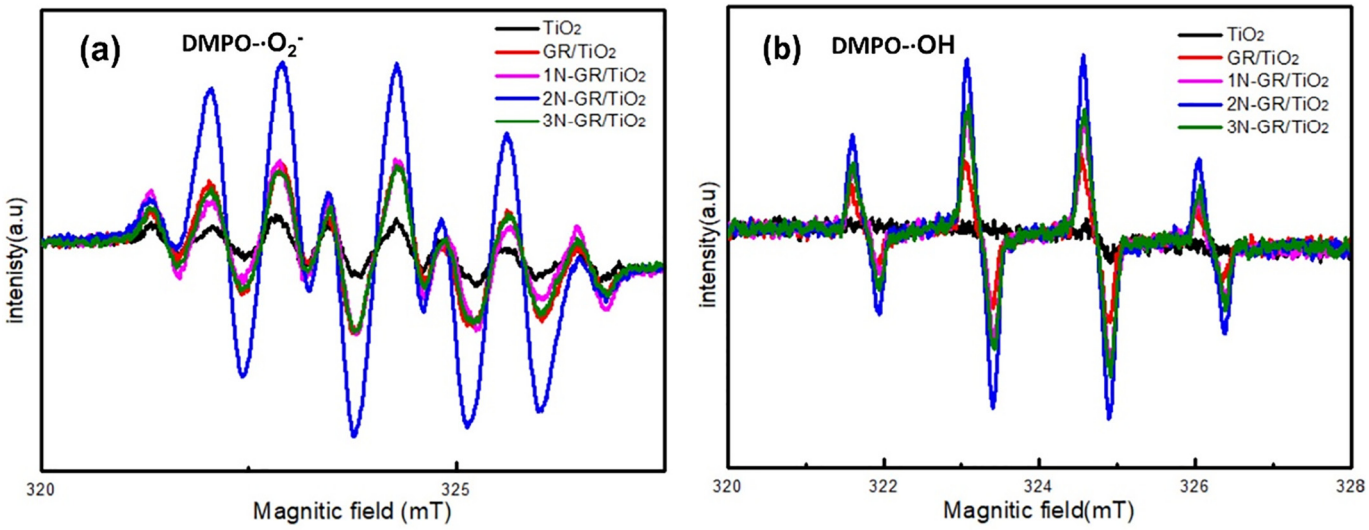

Fig. 8. (a) superoxide radicals (·O_2^-) and (b) hydroxyl radical (·OH) detection of pristine TiO_2 and GR/TiO_2, 1 N-GR/TiO_2, 2 N-GR/TiO_2, 3 N-GR/TiO_2.

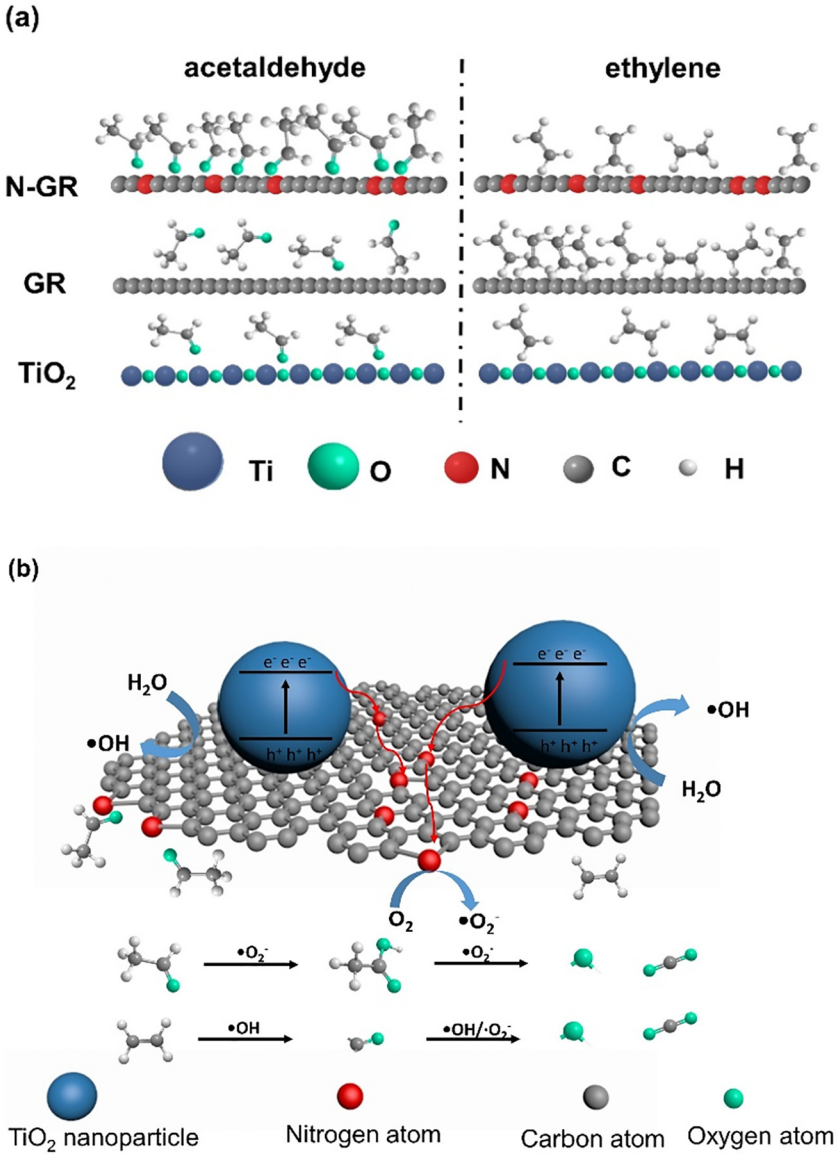

Fig. 9. (a) Schematic adsorption of N-GR (upper), GR (middle) and TiO_2 (bottom) towards acetaldehyde (left) and ethylene (right); (b) schematic structure of the N-GR/TiO_2 nanocomposite and the main process of photodegradation for acetaldehyde and ethylene.

4. Conclusions

In this work, nitrogen doped graphene/TiO_2 nanocomposites were synthesized by a simple heat treatment method. The properties of the composites were strongly influenced by doped nitrogen atoms. Attention was paid to the adsorption ability and the photocatalytic performance of the composites. Compared with pristine TiO_2 and GR/TiO_2, the N-GR/TiO_2 showed superior acetaldehyde adsorption ability and photocatalytic degradation efficiency, among which the 2 N-GR/TiO_2 sample showed the best photocatalytic performance. Different from acetaldehyde, adsorption capacity and removal efficiency towards ethylene reached the highest on the sample of GR/TiO_2 rather than N-GR/TiO_2. The reason could be assigned to two main aspects. For one reason, the polarity of graphene was enhanced by the doped nitrogen atoms. The polar molecules such as acetaldehyde preferred to adhere to polar structure (N-GR/TiO_2) while nonpolar molecules such as ethylene tended to be adsorbed to nonpolar structure (GR/TiO_2), which was demonstrated by adsorption of flowing gas and TPD graph. Besides, the amidogen introduced by pyrrolic nitrogen was conductive to the adsorption of acetaldehyde molecules while of no help to the adsorption of ethylene. For another reason, nitrogen doped graphene could provide sites for oxygen adsorption and could yield more $\cdot O_2^-$, which are important oxidizing agents for the degradation of acetaldehyde, whereas in the photodegradation of ethylene ·OH plays the crucial role. This work not only casts sight on the importance of adsorption for the photodegradation process, but also reveals that polarity plays a significant role on the adsorption of organic molecules.

Conflicts of interest

There are no conflicts to declare.

Acknowledgement

This work was financially supported by the National Key Research and Development Program of China (2016YFA0203000), the NSFC-DFG bilateral organization program (51761135107), the Youth Innovation Promotion Association CAS (2017042), the National Natural Science Foundation of China(41571130022) and Shanghai Sailing Program (18YF1426800).

References

[1] S. Wang, H.M. Ang, M.O. Tade, Volatile organic compounds in indoor environment and photocatalytic oxidation: state of the art, Environ. Int. 33 (2007) 694–705.
[2] A.H. Mamaghani, F. Haghighat, C.-S. Lee, Photocatalytic oxidation technology for indoor environment air purification: the state-of-the-art, Appl. Catal. B Environ. 203 (2017) 247–269.
[3] M. Bahri, F. Haghighat, S. Rohani, H. Kazemian, Impact of design parameters on the performance of non-thermal plasma air purification system, Chem. Eng. J. 302 (2016) 204–212.
[4] N.E. Klepeis, W.C. Nelson, W.R. Ott, J.P. Robinson, A.M. Tsang, P. Switzer, J.V. Behar, S.C. Hern, W.H. Engelmann, The National Human Activity Pattern Survey (NHAPS): a resource for assessing exposure to environmental pollutants, J. Expo. Anal. Environ. Epidemiol. 11 (2001) 231–252.
[5] V. Lannuque, M. Camredon, F. Couvidat, A. Hodzic, R. Valorso, S. Madronich, B. Bessagnet, B. Aumont, Exploration of the influence of environmental conditions on secondary organic aerosol formation and organic species properties using explicit simulations: development of the VBS-GECKO parameterization, Atmos. Chem. Phys. 18 (2018) 13411–13428.
[6] S. Wang, R. Wu, T. Berndt, M. Ehn, L. Wang, Formation of highly oxidized radicals and multifunctional products from the atmospheric oxidation of alkylbenzenes, Environ. Sci. Technol. 51 (2017) 8442–8449.
[7] Y. Chen, S. Tong, J. Wang, C. Peng, M. Ge, X. Xie, J. Sun, Effect of titanium dioxide on secondary organic aerosol formation, Environ. Sci. Technol. 52 (2018) 11612–11620.
[8] X. Ma, Q. Xiang, Y. Liao, T. Wen, H. Zhang, Visible-light-driven CdSe quantum dots/graphene/TiO2 nanosheets composite with excellent photocatalytic activity for E. coli disinfection and organic pollutant degradation, Appl. Surf. Sci. 457 (2018) 846–855.
[9] P. Wang, Y. Lu, X. Wang, H. Yu, Co-modification of amorphous-Ti(IV) hole cocatalyst and Ni(OH)2 electron cocatalyst for enhanced photocatalytic H2-production performance of TiO2, Appl. Surf. Sci. 391 (2017) 259–266.
[10] T. Sun, Y. Chen, X.-Q. Ma, Z. Li, H. Li, X.-L. Cui, Facile synthesis of visible light activated carbon-incorporated Mn doped TiO2 microspheres via flame thermal method, J. Inorg. Mater. 30 (2015) 1002–1008.
[11] Q. Tong, Y.-M. Dong, L. Yan, D.-N. He, High-efficient synthesis and photocatalytic properties of ag/AgBr/TiO2 monolithic photocatalysts using sodium alginate as substrate, J. Inorg. Mater. 32 (2017) 637–642.
[12] C.H. Ao, S.C. Lee, Combination effect of activated carbon with TiO2 for the photodegradation of binary pollutants at typical indoor air level, J. Photochem. Photobiol. A Chem. 161 (2004) 131–140.
[13] L. Zou, Y. Luo, M. Hooper, E. Hu, Removal of VOCs by photocatalysis process using adsorption enhanced TiO2-SiO(2)catalyst, Chem. Eng. Process. 45 (2006) 959–964.
[14] Y. Hu, X. Xie, X. Wang, Y. Wang, Y. Zeng, D.Y.H. Pui, J. Sun, Visible-light upconversion carbon quantum dots decorated TiO2 for the photodegradation of flowing gaseous acetaldehyde, Appl. Surf. Sci. 440 (2018) 266–274.
[15] Q. Zeng, X. Xie, X. Wang, Y. Wang, G. Lu, D.Y.H. Pui, J. Sun, Enhanced photocatalytic performance of Ag@TiO2 for the gaseous acetaldehyde photodegradation under fluorescent lamp, Chem. Eng. J. 341 (2018) 83–92.
[16] B.I. Stefanov, Z. Topalian, C.G. Granqvist, L. Osterlund, Acetaldehyde adsorption and condensation on anatase TiO2: influence of acetaldehyde dimerization, J. Photochem. Photobiol. A Chem. 381 (2014) 77–88.
[17] P. Thanh-Dong, B.-K. Lee, C.-H. Lee, The advanced removal of benzene from aerosols by photocatalytic oxidation and adsorption of Cu-TiO2/PU under visible light irradiation, Appl. Catal. B Environ. 182 (2016) 172–183.
[18] Y.-B. Zhao, L.-X. Sang, TiO2 nanoring/nanotube hierarchical structure growth mechanism and optical absorption property, J. Inorg. Mater. 32 (2017) 1327–1331.
[19] H.J. Lee, H.O. Seo, D.W. Kim, K.-D. Kim, Y. Luo, D.C. Lim, H. Ju, J.W. Kim, J. Lee, Y.D. Kim, A high-performing nanostructured TiO2 filter for volatile organic compounds using atomic layer deposition, Chem. Commun. 47 (2011) 5605–5607.
[20] A.Y. Chen, T.T. Zhang, Y.J. Qiu, D. Wang, P. Wang, H.J. Li, Y. Li, J.H. Yang, X.Y. Wang, X.F. Xie, Construction of nanoporous gold/g-C3N4 heterostructure for electrochemical supercapacitor, Electrochim. Acta 294 (2019) 260–267.
[21] Y.-F. Wang, C.-F. Peng, H.-P. Chao, Sorption of volatile organic compounds on organic substance-modified titanate nanotubes, Aerosol Air Qual. Res. 15 (2015) 2688–2699.
[22] M. Li, B. Lu, Q.-F. Ke, Y.-J. Guo, Y.-P. Guo, Synergetic effect between adsorption and photodegradation on nanostructured TiO2/activated carbon fiber felt porous composites for toluene removal, J. Hazard. Mater. 333 (2017) 88–98.
[23] C.H. Ao, S.C. Lee, Enhancement effect of TiO2 immobilized on activated carbon filter for the photodegradation of pollutants at typical indoor air level, Appl. Catal. B Environ. 44 (2003) 191–205.
[24] M. Xing, D. Qi, J. Zhang, F. Chen, B. Tian, S. Bagwas, M. Anpo, Super-hydrophobic fluorination mesoporous MCF/TiO2 composite as a high-performance photocatalyst, J. Catal. 294 (2012) 37–46.
[25] F. Batault, F. Thevenet, V. Hequet, C. Rillard, L. Le Coq, N. Locoge, Acetaldehyde and acetic acid adsorption on TiO2 under dry and humid conditions, Chem. Eng. J. 264 (2015) 197–210.
[26] Z. Shayegan, F. Haghighat, C.-S. Lee, A. Bahloul, M. Huard, Effect of surface fluorination of P25-TiO2 on adsorption of indoor environment volatile organic compounds, Chem. Eng. J. 346 (2018) 578–589.
[27] P. Thanh-Dong, B.-K. Lee, Selective removal of polar VOCs by novel photocatalytic activity of metals co-doped TiO2/PU under visible light, Chem. Eng. J. 307 (2017) 63–73.
[28] Y. Duan, L. Liang, K. Lv, Q. Li, M. Li, TiO2 faceted nanocrystals on the nanofibers: Homojunction TiO2 based Z-scheme photocatalyst for air purification, Appl. Surf. Sci. 456 (2018) 817–826.
[29] Y. Zhang, Z. Si, J. Gao, Y. Liu, L. Liu, X. Wu, R. Ran, D. Weng, Facile synthesis of NaOH-promoted Pt/TiO2 catalysts for toluene oxidation under visible light irradiation, Appl. Surf. Sci. 469 (2019) 246–252.
[30] H. Zhang, X. Lv, Y. Li, Y. Wang, J. Li, P25-graphene composite as a high performance photocatalyst, ACS Nano 4 (2010) 380–386.
[31] Q. Xiang, J. Yu, M. Jaroniec, Graphene-based semiconductor photocatalysts, Chem. Soc. Rev. 41 (2012) 782–796.
[32] X. Li, J. Yu, S. Wageh, A.A. Al-Ghamdi, J. Xie, Graphene in photocatalysis: a review, Small 12 (2016) 6640–6696.
[33] W. Lin, X. Xie, X. Wang, Y. Wang, D. Segets, J. Sun, Efficient adsorption and sustainable degradation of gaseous acetaldehyde and o-xylene using rGO-TiO 2 photocatalyst, Chem. Eng. J. 349 (2018) 708–718.
[34] L.Y. Lin, Y. Nie, S. Kavadiya, T. Soundappan, P. Biswas, N-doped reduced graphene oxide promoted nano TiO2 as a bifunctional adsorbent/photocatalyst for CO2 photoreduction: effect of N species, Chem. Eng. J. 316 (2017) 449–460.
[35] Y. Xu, Y. Mo, J. Tian, P. Wang, H. Yu, J. Yu, The synergistic effect of graphitic N and pyrrolic N for the enhanced photocatalytic performance of nitrogen-doped graphene/TiO2 nanocomposites, Appl. Catal. B Environ. 181 (2016) 810–817.
[36] Z. Mou, Y. Wu, J. Sun, P. Yang, Y. Du, C. Lu, TiO2 nanoparticles-functionalized N-doped graphene with superior interfacial contact and enhanced charge separation for photocatalytic hydrogen generation, ACS Appl. Mater. Interfaces 6 (2014) 13798–13806.
[37] M. Guo, D. Li, M. Zhao, Y. Zhang, D. Geng, A. Lushington, X. Sun, Nitrogen ion implanted graphene as thrombo-protective safer and cytoprotective alternative for biomedical applications, Carbon 61 (2013) 321–328.
[38] D. Wei, Y. Liu, Y. Wang, H. Zhang, L. Huang, G. Yu, Synthesis of N-doped graphene by chemical vapor deposition and its electrical properties, Nano Lett. 9 (2009) 1752–1758.
[39] M. Wu, C. Cao, J.Z. Jiang, Light non-metallic atom (B, N, O and F)-doped graphene: a first-principles study, Nanotechnology 21 (2010).
[40] Y. Zhang, K. Fugane, T. Mori, L. Niu, J. Ye, Wet chemical synthesis of nitrogen-doped graphene towards oxygen reduction electrocatalysts without high-temperateure pyrolysis, J. Mater. Chem. 22 (2012) 6575–6580.
[41] B. Liu, E.S. Aydil, Growth of oriented single-crystalline rutile TiO2 nanorods on transparent conducting substrates for dye-sensitized solar cells, J. Am. Chem. Soc. 131 (2009) 3985–3990.
[42] Y. Zhou, Q. Bao, L.A.L. Tang, Y. Zhong, K.P. Loh, Hydrothermal dehydration for the "Green" reduction of exfoliated graphene oxide to graphene and demonstration of tunable optical limiting properties, Chem. Mater. 21 (2009) 2950–2956.
[43] Y. Li, Y. Zhao, H. Cheng, Y. Hu, G. Shi, L. Dai, L. Qu, Nitrogen-doped graphene quantum dots with oxygen-rich functional groups, J. Am. Chem. Soc. 134 (2012) 15–18.
[44] M. Favaro, S. Agnoli, C. Di Valentin, C. Mattevi, M. Cattelan, L. Artiglia, E. Magnano, F. Bondino, S. Nappini, G. Granozzi, TiO2/graphene nanocomposites from the direct reduction of graphene oxide by metal evaporation, Carbon 68 (2014) 319–329.
[45] H. Irie, Y. Watanabe, K. Hashimoto, Carbon-doped anatase TiO2 powders as a visible-light sensitive photocatalyst, Chem. Lett. 32 (2003) 772–773.
[46] Q. Cheng, Y. Liao, Q. Wang, Y. Sun, M. Chen, Synthesis of nitrogen-connected beta-amidogen thiazole ring by reacting aldehyde, thiazole and diester malonate in alkaline catalyst-pot, carrying out alkali hydrolysis, acidification and decarboxylation, distilling solvent and washing, in, Huaihai Inst Technology.
[47] A. Hao, Y. Zhang, C. Zheng, H. Zheng, Formaldehyde Removing Agent Comprises Main Material Namely, Amidogen Type- or Ester Type-Compound, and Retanning Filling Agent, Adsorbent, Surfactant, pH Regulating Agent and Reducing Agent, in, Beijing Fanbo Sci & Technology Co Ltd.
[48] R. Salcedo, M. Bosquez, Schiff base complexes that form sandwich compounds, J. Mol. Model. 24 (2018).
[49] M.A. Hassan, A.M. Omer, E. Abbas, W.M.A. Baset, T.M. Tamer, Preparation, physicochemical characterization and antimicrobial activities of novel two phenolic chitosan Schiff base derivatives, Sci. Rep. 8 (2018).
[50] N. Keller, M.-N. Ducamp, D. Robert, V. Keller, Ethylene removal and fresh product storage: a challenge at the frontiers of chemistry. Toward an approach by photocatalytic oxidation, Chem. Rev. 113 (2013) 5029–5070.
[51] M.L.V. de Chiara, S. Pal, A. Licciulli, M.L. Amodio, G. Colelli, Photocatalytic degradation of ethylene on mesoporous TiO2/SiO2 nanocomposites: effects on the ripening of mature green tomatoes, Biosyst. Eng. 132 (2015) 61–70.
[52] Q. Zhang, S. Ye, X. Chen, X. Song, L. Li, X. Huang, Photocatalytic degradation of ethylene using titanium dioxide nanotube arrays with Ag and reduced graphene oxide irradiated by gamma-ray radiolysis, Appl. Catal. B Environ. 203 (2017) 673–683.
[53] F. Meng, J. Li, S.K. Cushing, M. Zhi, N. Wu, Solar hydrogen generation by nanoscale p-n junction of p-type molybdenum disulfide/n-type nitrogen-doped reduced graphene oxide, J. Am. Chem. Soc. 135 (2013) 10286–10289.
[54] Y. Hou, Z. Wen, S. Cui, X. Guo, J. Chen, Constructing 2D porous graphitic C3N4 nanosheets/nitrogen-doped graphene/layered MoS2 ternary nanojunction with enhanced photoelectrochemical activity, Adv. Mater. 25 (2013) 6291–6297.
[55] L. Ferrighi, M. Datteo, G. Fazio, C. Di Valentin, Catalysis under cover: enhanced reactivity at the interface between (doped) graphene and anatase TiO2, J. Am. Chem. Soc. 138 (2016) 7365–7376.
[56] Y. Nosaka, A.Y. Nosaka, Generation and detection of reactive oxygen species in photocatalysis, Chem. Rev. 117 (2017) 11302–11336.
[57] Z. Li, Y. Luan, Y. Qu, L. Jing, Modification strategies with inorganic acids for efficient photocatalysts by promoting the adsorption of O-2, ACS Appl. Mater.

Interfaces 7 (2015) 22727–22740.
[58] L. He, L. Jing, Y. Luan, L. Wang, H. Fu, Enhanced visible activities of alpha-Fe2O3 by coupling N-doped graphene and mechanism insight, ACS Catal. 4 (2014) 990–998.
[59] X. Niu, Y. Li, H. Shu, J. Wang, Revealing the underlying absorption and emission mechanism of nitrogen doped graphene quantum dots, Nanoscale 8 (2016) 19376–19382.
[60] T. Ochiai, A. Fujishima, Photoelectrochemical properties of TiO2 photocatalyst and its applications for environmental purification, J. Photochem. Photobiol. C Photchem. Rev. 13 (2012) 247–262.
[61] M.A. Henderson, A surface science perspective on TiO2 photocatalysis, Surf. Sci. Rep. 66 (2011) 185–297.
[62] L.-Y. Lin, Y. Nie, S. Kavadiya, T. Soundappan, P. Biswas, N-doped reduced graphene oxide promoted nano TiO2 as a bifunctional adsorbent/photocatalyst for CO2 photoreduction: effect of N species, Chem. Eng. J. 316 (2017) 449–460.
[63] G. Williams, B. Seger, P.V. Kamat, TiO2-graphene nanocomposites. UV-assisted photocatalytic reduction of graphene oxide, ACS Nano 2 (2008) 1487–1491.
[64] B. Hauchecorne, T. Tytgat, S.W. Verbruggen, D. Hauchecorne, D. Terrens, M. Smits, K. Vinken, S. Lenaerts, Photocatalytic degradation of ethylene: an FTIR in situ study under atmospheric conditions, Appl. Catal. B Environ. 105 (2011) 111–116.
[65] D.R. Park, J.L. Zhang, K. Ikeue, H. Yamashita, M. Anpo, Photocatalytic oxidation of ethylene to CO2 and H2O on ultrafine powdered TiO2 photocatalysts in the presence of O-2 and H2O, J. Catal. 185 (1999) 114–119.
[66] S. Yamazaki, S. Tanaka, H. Tsukamoto, Kinetic studies of oxidation of ethylene over a TiO2 photocatalyst, J. Photochem. Photobiol. A Chem. 121 (1999) 55–61.